Stability boundaries for the Rayleigh-Taylor instability in accelerated elastic-plastic solid slabs

A. R. Piriz* and S. A. Piriz
Instituto de Investigaciones Energéticas (INEI), E.T.S.I.I., and CYTEMA, Universidad de Castilla-La Mancha, 13071 Ciudad Real, Spain

N. A. Tahir
GSI Helmholtzzentrum für Schwerionenforschung Darmstadt, Planckstrasse 1, 64291 Darmstadt, Germany

(Received 18 September 2019; published 12 December 2019; corrected 10 January 2020)

The linear theory of the incompressible Rayleigh-Taylor instability in elastic-plastic solid slabs is developed on the basis of the simplest constitutive model consisting in a linear elastic (Hookean) initial stage followed by a rigid-plastic phase. The slab is under the action of a constant acceleration, and it overlays a very thick ideal fluid. The boundaries of stability and plastic flow are obtained by assuming that the instability is dominated by the average growth of the perturbation amplitude and neglecting the effects of the higher oscillation frequencies during the stable elastic phase. The theory yields complete analytical expressions for such boundaries for arbitrary Atwood numbers and thickness of the solid slabs.

DOI: 10.1103/PhysRevE.100.063104

I. INTRODUCTION

The interest on the Rayleigh-Taylor instability (RTI) in accelerated solids has grown considerably since the first theoretical analysis by Miles in 1966 because of its relevance in many physical scenarios [1–53]. It is central to a wide variety of experiments on high-energy-density (HED) physics involving the implosion of spherical and cylindrical solid shells, which includes the different approaches to inertial confinement fusion, as well as the acceleration of planar plates [54–59].

There are at present a significant number of methods to drive these experiments in different geometries and regimes that include the use of high explosives (HEs) either detonated in close contact with the solid plate or shell [52,53] or by allowing a separation gap in order to ensure a gentler acceleration of the solid by the detonation products [3,7]. A similar explosion effect can also be produced by heating a reservoir with a strong shock driven by an intense laser pulse [19,23,24,27,33,34]. In addition, the ablation process induced by thermal radiation has also been used for the acceleration of planar slabs by generating a slowly rising pressure pulse that prevents the shock formation [19,24]. Pulse shaping is also possible with the magnetic pressure generated by intense pulsed electrical currents, which allows for the acceleration of solids slabs without complete melting [20–22]. More recently a new approach has been proposed based on the use of an intense heavy ion beam pulse which heats the absorber region surrounding a cylindrical shell, which is thus accelerated inwards by the absorber expansion in a process that somewhat resembles the implosions driven by HEs [60–70].

In addition, RTI in elastic-plastic (EP) solids seems to play a role in geophysical processes related to Earth plate tectonics by participating in the removal of portions of the mantle lithosphere through a dynamical interaction taking place at the interface between the lithosphere and the underlying mantle [36,37]. RTI in solids could also be relevant in the crust of neutron stars [10,11], and it may trigger the onset of starquakes in the strongly magnetized neutron stars known as magnetars [47,49,50].

A distinguishing characteristic of RTI in EP solids is the dependence of the stability conditions on the initial perturbation amplitude ξ_0 in addition to the perturbation wavelength λ, so that both of them control the stability boundaries. The first indication of this singular trait came from the pioneer experiments by Barnes *et al.* [3,7]. But it was Drucker who first realized that at least some of those experimental results had to be interpreted in terms of the influence of the initial perturbation amplitude [5,6]. This issue finally became clear after the extensive two-dimensional (2D) numerical simulations performed by Swegle and Robinson showing stability maps in the space (ξ_0, λ) that determine the stability boundaries for the RTI in EP solids [8,9]. However, it was difficult to discern from those simulations the physical mechanisms underlying such behavior, mainly because of the complexities of the physical conditions present in the numerical simulations arising from the existence of an initial phase dominated by the shock-driven Richtmyer-Meshkov instability and from the transient character of the pressure driving the slab acceleration, as well as from the previous transient phase that takes place before the slab is accelerated as a whole.

To shed some light on the physical process determining these stability maps, Nizovtzev and Raevskii [12–15] developed an heuristic model in which they assumed that plastic flow was the only requirement for the onset of the instability. This assumption was put in doubt by Terrones [30], and it was later shown by Piriz *et al.* [31,32] that plastic flow was a necessary but not sufficient condition for the instability. In any case, leaving aside the "correction factor" introduced

*roberto.piriz@uclm.es

by Nizovtzev and Raevskii with the only purpose to fit the Drucker's stability criterion, their model would actually be appropriate for estimating the boundary of the transition from the RTI phase dominated by the elasticity to the phase dominated by the plastic flow (EP transition).

The most recent studies of the stability boundaries were performed by Piriz *et al.* [31,32,38,39] for semi-infinite media on the basis of an approximate irrotational model for the evolution of the instability during the elastic phase. Extensive comparisons with 2D numerical simulations have shown an excellent agreement with this relatively simple model. But, unfortunately, the basic assumption of irrotational elastic flow does not hold anymore when the more realistic case of finite thickness media is considered [46,47].

It seems to exist an implicit but rather common belief that in realistic situations involving EP solids the initial elastic phase is so short that its effects should be irrelevant for the subsequent evolution of the instability. Such a prejudice, such as happened in the past with the belief that plastic flow was a sufficient condition for instability, seems to have interfered with the progress in the understanding of the RTI in EP solids. However, as was shown in Refs. [31,32] and as will also be shown in the present work for arbitrary slab thicknesses, regardless of how short the elastic phase can be, it cannot be avoided. And it is just such a phase that actually governs the dependence of the maximum stable initial perturbation amplitude with the perturbation wavelength, which is the main characteristic of the stability boundaries for the RTI in EP solids. As a consequence, these boundaries depend not only on the solid yield strength Y controlling the instability after plastic flow, but also have to depend on the shear modulus G that controls it during the early elastic phase.

Certainly, the relevance of this initial elastic phase can be seen as a quite unfortunate feature for the design of experiments on HED physics because a criterion based only on the initial perturbation amplitude would allow for conceiving completely stable experiments provided that a sufficiently good surface finish of the solid slab is ensured, irrespective of the wavelength spectrum of the perturbations. As we will see later, at least some of such an ideal situation could still be possible in some particular cases. In fact, as has been already shown by the theory, in the situations in which the Atwood number is $A_T < 1$, there exists an instability threshold for the elastic RTI below which the slab turns out to be stable for any perturbation wavelength [10,11,47,49,50]. That is, below this threshold only an amplitude criterion should, in fact, be satisfied in order to ensure total stability. However, the requirement of $A_T < 1$ may considerably restrict the possible means to drive the slab or shell acceleration. As far as we are aware, the only way at present to have such a situation is by means of HEs in direct contact with the shell to be accelerated [53].

However, the foreseen experiments in the Laboratory of Planetary Sciences (LAPLAS) driven by an intense heavy ion beam to be realized at the future Facility for Ion and Antiproton Research (FAIR), presently under construction at the GSI Helmholtzzentrum für Schwerionenforschung Darmstadt (Germany) [60–70], will share this characteristic with the HE experiments of Ref. [53]. In fact, the role of the HEs is played in LAPLAS by the annular absorber region, which surrounds the cylindrical shell, where part of the beam energy is volumetrically deposited leading to its expansion and to the consequent implosion of the internal shell. Extensive 2D numerical simulations have shown that the maximum Atwood number is $A_T^{\max} \approx 0.4$ [67–70]. This feature is expected to convert LAPLAS into a rather unique tool for the study of the physics of HED matter.

II. INSTABILITY LINEAR ANALYSIS

We consider the 2D situation schematically represented in Fig. 1 in which a solid slab of density ρ_2 and thickness h overlays an ideal fluid of density $\rho_1 < \rho_2$ that occupies the semispace $y \geqslant 0$. The slab is assumed to be an ideal elastic-plastic solid occupying the region $-h \leqslant y \leqslant 0$ that is characterized by a shear modulus G and a yield strength Y [31]. The region above the slab ($y \leqslant -h$) is assumed to be empty or filled with a very tenuous ideal gas of density $\rho_3 \ll \rho_1$. The whole system is under the action of a uniform gravity acceleration $\boldsymbol{g} = g\boldsymbol{e_y} = -\nabla\varphi$ ($\boldsymbol{e_y}$ is the unitary vector in the vertical direction and φ is the gravitational potential). The media are also assumed to be incompressible and immiscible.

The analysis starts with the continuous media equations for the conservation of mass and momentum:

$$\frac{d\rho_n}{dt} + \rho_n \frac{\partial v_{ni}}{\partial x_i} = 0, \tag{1}$$

$$\rho_n \frac{dv_{ni}}{dt} = -\frac{\partial p_n}{\partial x_i} + \rho_n g_i + \frac{\partial \sigma_{ik}^{(n)}}{\partial x_k}, \tag{2}$$

where $n = 1, 2, 3$ refer, respectively, to the bottom, middle, and top regions, and we have used index notation for Cartesian vectors and tensors so that $i = 1, 2, 3$ indicate the space coordinates x, y, z, and $g_i = g$ for $i \equiv y$ and $g_i = 0$ otherwise. In addition, v_{ni}, ρ_n, and p_n are, respectively, the ith velocity component, density, and pressure; and $\sigma_{ik}^{(n)}$ is the deviatoric part of the stress tensor $\Sigma_{ik}^{(n)} = -p_n\delta_{ik} + \sigma_{ik}^{(n)}$ of the medium n (δ_{ik} is the Kronecker δ). We will interchange vector and index notation to the best convenience of the presentation. On the other hand, dM/dt represents the material derivative of a

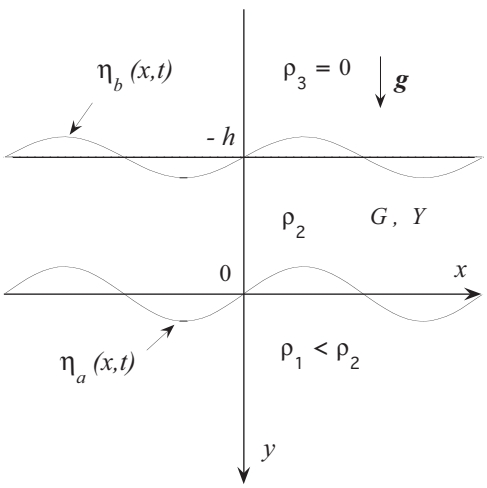

FIG. 1. Schematic of the two-interfaces system formed by the elastic-plastic slab on the top of a semi-infinite ideal fluid.

magnitude M:

$$\frac{dM}{dt} = \frac{\partial M}{\partial t} + v_{ni}\frac{\partial M}{\partial x_i} = 0. \tag{3}$$

Following Refs. [47,50] we linearize the previous equations by expressing every magnitude M as $M = M_0 + \delta M$, where M_0 corresponds to the equilibrium value of M and $\delta M \ll M_0$ is its perturbation. Then, by assuming incompressible perturbations ($\delta\rho_n = 0$), we get the linearized equations for mass and momentum conservation:

$$\frac{\partial(\delta v_{ni})}{\partial x_i} = 0, \tag{4}$$

$$\rho_n\frac{\partial(\delta v_{ni})}{\partial t} = -\frac{\partial(\delta p_n + \rho_n\delta\varphi_n)}{\partial x_i} + \frac{\partial S_{ik}^{(n)}}{\partial x_k}, \tag{5}$$

where $\delta\varphi_n = -\rho_n g\eta_{ny}$ (η_{ny} is the vertical component of the displacement $\boldsymbol{\eta_n}$, and $\dot{\boldsymbol{\eta}}_{\boldsymbol{n}} = \delta\boldsymbol{v_n}$), and we have defined $\delta\sigma_{ik}^{(n)} \equiv S_{ik}^{(n)}$. For the ideal media ($n = 1, 3$), we have $S_{ik}^{(1)} = S_{ik}^{(3)} = 0$, and for the elastic-plastic slab, we assume as in Refs. [31,32] the nonlinear Prandtl-Reuss model for which the solid behaves like a perfectly elastic Hookean (linear) solid for the smaller strains, and it behaves like a rigid-plastic solid otherwise. Thus, in the elastic phase, we have

$$\frac{\partial S_{ik}^{(2)}}{\partial t} = 2G\dot{e}_{ik}, \quad e_{ik} = \frac{1}{2}\left[\frac{\partial(\delta\eta_{2i})}{\partial x_k} + \frac{\partial(\delta\eta_{2k})}{\partial x_i}\right], \tag{6}$$

where the upper dot indicates time derivative and e_{ik} is the strain tensor.

For the plastic phase we write [31,32,71]

$$S_{ik}^{(2)} = \sqrt{\frac{2}{3}}\frac{\dot{e}_{ik}}{\|\dot{e}_{ik}\|}\beta Y, \tag{7}$$

where $\beta > 1$ is a numerical factor that modifies the usual von Mises criterion for taking into account the fact observed by Drucker [5,6] that, in order to consider the instability of the system, it is necessary that it has already overcome the intermediate phase of contained plastic flow determined by the usual von Mises flow criterion. Therefore, we will assume here that the transition to the regime in which RTI is controlled by the plastic flow occurs when the phase of unrestricted plastic flow has been achieved. As discussed in Ref. [72], during the intermediate phase of contained plastic flow above mentioned, the elastic action still plays a major role and, in practice, it can be considered as part of the initial elastic phase. We will come back later to this point.

A. Displacement field and growth rate in the elastic phase

The velocity field in the asymptotic regime and the instability growth rate for the RTI in a finite thickness elastic medium overlying a semi-infinite ideal medium were obtained in Ref. [47]. Here we will summarize those results, and we will present them in a somewhat different manner more appropriate for deriving the differential equations for the motion of the interfaces at $y = 0$ and $y = -h$. Then, as in Ref. [47], we use the Helmholtz decomposition, but here we write it for the displacement field during the elastic phase [73,74]:

$$\boldsymbol{\eta}_2 = \boldsymbol{\nabla}\phi_2 + \boldsymbol{\nabla}\times(\psi_2\boldsymbol{e}_z), \tag{8}$$

where ϕ_2 and $\boldsymbol{\psi_2} = \psi_2\boldsymbol{e}_z$ are, respectively, the Lamé scalar and vector potentials functions.

After substitution of Eq. (8) into Eqs. (4) and (5), we get

$$\nabla^2\phi_n = 0, \tag{9}$$

$$\boldsymbol{\nabla}\left(\frac{\partial^2\phi_n}{\partial t^2} + \frac{\delta p_n}{\rho_n} + \delta\varphi_n\right) + \boldsymbol{\nabla}\times\left[\frac{\partial^2\psi_n}{\partial t^2} - \frac{G}{\rho_n}\nabla^2(\psi_n\boldsymbol{e}_z)\right] = 0, \tag{10}$$

where for the ideal medium in the region $y \geqslant 0$ it is $\psi_1 = 0$.

As is well known, there is a degree of freedom that allows us to choose the potentials ϕ_n and $\boldsymbol{\psi_n}$ such that they are solutions of the equations system formed by Eq. (9) and the two following ones [73,74]:

$$\rho_n\frac{\partial^2\phi_n}{\partial t^2} + \delta p_n - \rho_n g\eta_{ny} = 0, \tag{11}$$

$$\rho_2\frac{\partial^2\psi_2}{\partial t^2} = G\nabla^2\psi_2. \tag{12}$$

By considering 2D perturbations, we can write the following convenient expressions for the potential functions in the region $-h \leqslant y \leqslant 0$ [47,49,50]:

$$\phi_2 = \frac{a\cosh ky + b\cosh k(h+y)}{\sinh kh}\sin kx, \tag{13}$$

$$\psi_2 = \frac{c\sinh \ell y + d\sinh \ell(h+y)}{\sinh \ell h}\cos kx, \tag{14}$$

where $k = 2\pi/\lambda$ is the perturbation wave number,

$$\ell = \sqrt{k^2 + \frac{\gamma_{ei}^2\rho_2}{G}}, \tag{15}$$

and a, b, c, and d are time functions such that

$$a \propto b \propto c \propto d \propto F(t) = \sum_i Q_i e^{\gamma_{ei}t}, \tag{16}$$

with Q_i being constants, and γ_{ei} the growth rate that will be determined by the boundary conditions on both interfaces. In addition, the potential ϕ_1 associated to the displacement field in the region $y \geqslant 0$ reads ($\psi_1 = 0$)

$$\phi_1 = a_1 e^{-ky}\sin kx,\ a_1 \propto F(t). \tag{17}$$

In order to find all the possible values of the growth rate γ_{ei} we impose boundary conditions on the velocities and the stresses at $y = 0$ and $y = -h$. Namely, we have [47,50]

$$\delta v_{1y}(0) = \delta v_{2y}(0) = \dot{\eta}_a(x,t),\ \delta v_{2y}(-h) = \dot{\eta}_b(x,t), \tag{18}$$

$$-\delta p_1(0) = -\delta p_2(0) + S_{yy}^{(2)}(0), \tag{19}$$

$$-\delta p_2(-h) + S_{yy}^{(2)}(-h) = 0, \tag{20}$$

$$S_{xy}^{(2)}(0) = S_{xy}^{(2)}(-h) = 0, \tag{21}$$

where

$$\eta_a(x,t) = \eta_{2y}(0) = \xi_a(t)\sin kx, \tag{22}$$

$$\eta_b(x,t) = \eta_{2y}(-h) = \xi_b(t)\sin kx, \tag{23}$$

and δp_n ($n = 1, 2$) are given by Eq. (11). Equations (18) and (21) yield [47,50]

$$\dot{a}_1 = -(\dot{b} + \dot{d}), \tag{24}$$

$$c = -\frac{2k^2}{\ell^2 + k^2}a, \quad d = -\frac{2k^2}{\ell^2 + k^2}b, \tag{25}$$

$$k\dot{a} = -\frac{\ell^2 + k^2}{\ell^2 - k^2}\dot{\xi}_b, \quad k\dot{b} = \frac{\ell^2 + k^2}{\ell^2 - k^2}\dot{\xi}_a. \tag{26}$$

On the other hand, Eqs. (19) and (20) lead to the following forms for the momentum balance at $y = 0$ and $y = -h$, respectively:

$$\rho_2\left(\ddot{\xi}_a \coth kh - \frac{\ddot{\xi}_b}{\sinh kh}\right) + S'_{yy}(0) = \rho_2 kg\xi_a - \rho_1(\ddot{\xi}_a + kg\xi_a), \tag{27}$$

$$\rho_2\left(-\ddot{\xi}_b \coth kh + \frac{\ddot{\xi}_a}{\sinh kh}\right) + S'_{yy}(-h) = \rho_2 kg\xi_b, \tag{28}$$

where

$$S'_{yy}(0) = 2k^2G\left\{\frac{\ddot{\xi}_a - \ddot{\xi}_{a0}}{\gamma_{ei}^2}\coth kh - \frac{\ddot{\xi}_b - \ddot{\xi}_{b0}}{\gamma_{ei}^2 \sinh kh} + \frac{\ell^2 + k^2}{\ell^2 - k^2}\left[(\xi_a - \xi_0)\coth kh - \frac{\xi_b}{\sinh kh}\right] - \frac{2k\ell}{\ell^2 - k^2}\left[(\xi_a - \xi_0)\coth \ell h - \frac{\xi_b}{\sinh \ell h}\right]\right\}, \tag{29}$$

$$S'_{yy}(-h) = 2k^2G\left\{-\frac{\ddot{\xi}_b - \ddot{\xi}_{b0}}{\gamma_{ei}^2}\coth kh + \frac{\ddot{\xi}_a - \ddot{\xi}_{a0}}{\gamma_{ei}^2 \sinh kh} + \frac{\ell^2 + k^2}{\ell^2 - k^2}\left[-\xi_b \coth kh + \frac{(\xi_a - \xi_0)}{\sinh kh}\right] - \frac{2k\ell}{\ell^2 - k^2}\left[-\xi_b \coth \ell h + \frac{(\xi_a - \xi_0)}{\sinh \ell h}\right]\right\}. \tag{30}$$

By performing the time integral of Eq. (6) we have imposed that the displacement field $\boldsymbol{\eta}(x, y, t)$ be irrotational at $t = 0$ in order to ensure initially stress free conditions in the solid slab ($\psi_2(t = 0) = 0$). Since $\boldsymbol{\eta}(x, y, t)$ is a rotational field for $t > 0$, the expressions for S'_{yy} in Eqs. (27) and (28) include a dynamical component given by the first two terms of Eqs. (29) and (30) containing the accelerations $\ddot{\xi}_a$ and $\ddot{\xi}_b$, which will contribute to the total loading leading to plastic flow. It may worth noticing that when $S'_{yy}(0) = S'_{yy}(-h) = 0$, Eqs. (27) and (28) reduce to the equations found by Goncharov *et al.* for the case of a finite thickness ideal medium [75].

In addition, we have taken the following initial conditions (at $t = 0$):

$$\xi_a(0) = \xi_0, \quad \xi_b(0) = 0, \quad \dot{\xi}_a(0) = \dot{\xi}_b(0) = 0, \quad \ddot{\xi}_a(0) = \ddot{\xi}_{a0}, \quad \ddot{\xi}_b(0) = \ddot{\xi}_{b0}. \tag{31}$$

The solutions of the differential equations given by Eqs. (27) to (30) can be found in the usual manner by proposing an exponential form $\xi_a \propto \xi_b \propto e^{\gamma_{ei}t}$ for the homogeneous equations and adding to it a particular solution.

Introducing this exponential form into the homogeneous parts of Eqs. (27) and (28), we can easily see that the asymptotic equations obtained in Ref. [47] are retrieved [Eqs. (30) and (28) in that reference, respectively].

Therefore, all the possible values γ_{ei} of the growth rate are given by the dispersion relation such as it was found in Ref. [47]:

$$\begin{aligned}(2\kappa^2 + \sigma^2)^4 + 16\kappa^6(\kappa^2 + \sigma^2) - 8\kappa^3\sqrt{\kappa^2 + \sigma^2}(2\kappa^2 + \sigma^2)^2 \\ \times [\coth \alpha\kappa \coth \alpha\sqrt{\kappa^2 + \sigma^2} \\ - \operatorname{csch} \alpha\kappa \operatorname{csch} \alpha\sqrt{\kappa^2 + \sigma^2}] \\ = \kappa^2\sigma^4 - \frac{1 - A_T}{1 + A_T}\sigma^2(\kappa + \sigma^2)[\kappa\sigma^2 + (2\kappa^2 + \sigma^2)^2 \coth \alpha\kappa \\ - 4\kappa^3\sqrt{\kappa^2 + \sigma^2}\coth \alpha\sqrt{\kappa^2 + \sigma^2}],\end{aligned} \tag{32}$$

where the following dimensionless magnitude have been introduced:

$$\kappa = \frac{k}{k_0}, \quad \sigma = \frac{\gamma_{ei}}{\sqrt{k_0 g}}, \quad k_0 = \frac{\rho_2 g}{G}, \quad \alpha = \frac{\rho_2 gh}{G}, \quad A_T = \frac{\rho_2 - \rho_1}{\rho_2 + \rho_1}. \tag{33}$$

As was shown in Ref. [47], Eq. (32) is a transcendental equation for σ^2 as a function of κ with α and A_T as parameters, and σ^2 is always a real number. Furthermore, Eq. (32) has a unique real and positive root for $\kappa \leqslant \kappa_c$ [17,47,50], where $\kappa_c = k_c/k_0$ is the dimensionless cutoff wave number, for which $\sigma^2 = 0$, that is given by the following expression [47]:

$$\frac{2A_T}{1 + A_T}\alpha^2 - \frac{1 - A_T}{1 + A_T}\frac{w(2w + \sinh 2w)}{\sinh^2 w}\alpha - 4w^2\left[1 - \left(\frac{w}{\sinh w}\right)^2\right] = 0, \tag{34}$$

where $w = k_c h = \alpha\kappa_c$.

Instead, for $\kappa \geqslant \kappa_c$ when the system is stable and $\sigma^2 < 0$, Eq. (32) has an infinite number of roots [17], and the general solutions of the homogeneous parts of Eqs. (27) and (28) are given by the linear combination of the solutions corresponding to each one of these roots. Then the summation in Eq. (16) extends to infinity, and the general solution for $\kappa \geqslant \kappa_c$ consists in a multimodal oscillation [30].

B. Growth rate in the plastic phase

Since for the plastic phase we are assuming classical plasticity, the displacement field in this phase must be irrotational [76]. Then the Lamé potentials now will be given by Eqs. (13) and (17), and it will be $\psi_2 = 0$. On the other hand, the boundary conditions to be satisfied are still given by Eqs. (18) to (21).

In addition, as was discussed by Drucker [5], as well as in the books by Chen [72,77], we need to take into account that between the purely elastic phase and the late phase of unrestricted flow (plastic collapse), there is an intermediate stage of contained flow in which the elastic effects still play a major role. A description including such an intermediate phase is far too complicated and of no value for practical applications. Furthermore, the evolution of the RTI after the

initial elastic phase can be expected to be governed by the late phase of plastic collapse, such as happens in most of the problems in soil mechanics [72,77]. In this regard, the methods of limit analysis can be suitable for describing the plastic phase evolution of the instability.

Following Drucker and the methods of the limit analysis, we take the average of Eqs. (19) and (20) over half a wavelength and consider the sinusoidal perturbations at each interface like a set of bumps of height twice the perturbation amplitudes. Thus, such equations reduce to the following system for the momentum balance at $y = 0$ and $y = -h$, respectively:

$$\rho_2\left(\ddot{\xi}_a \coth kh - \frac{\ddot{\xi}_b}{\sinh kh}\right) + 2Yk = \rho_2 kg\xi_a - \rho_1(\ddot{\xi}_a + kg\xi_a), \tag{35}$$

$$\rho_2\left(-\ddot{\xi}_b \coth kh + \frac{\ddot{\xi}_a}{\sinh kh}\right) + 2Yk = \rho_2 kg\xi_b, \tag{36}$$

where we have considered that the unrestricted plastic flow occurs when the loading at the bottom level of the interface (the valleys) averaged over half a wavelength is $(1+\pi/2)Y(\lambda/2)$ [5,6,72,77], and that $(2/k)\int_0^{\pi} \sin u\ du = (4/\pi)(\lambda/2)$, with $(1+\pi/2)(\pi/4) \approx 2$.

As in the case of the equations for the elastic phase, the general solutions of Eqs. (35) and (36) can be written each one as the sum of the solution of the homogeneous equation plus a particular solution. And, once again, the solutions for the homogeneous equations can be found by proposing an exponential form: $\xi_a \propto \xi_b \propto e^{\gamma_{pi}}$, where γ_{pi} is the corresponding growth rate for the plastic phase and is given by the solutions of the following dispersion relation corresponding to an ideal fluid slab [50,75,78]:

$$\left(\frac{\kappa}{\sigma_p^2}\right)^2 - 1 = \left(\frac{\kappa}{\sigma_p^2} + 1\right)\frac{1-A_T}{1+A_T}\left(\frac{\kappa}{\sigma_p^2} + \coth \alpha\kappa\right), \tag{37}$$

where we have used the dimensionless magnitudes defined in Eq. (33). As is evident, this equation has two roots for σ_p^2:

$$\sigma_{p1}^2 = \frac{2A_T\kappa}{1+A_T+(1-A_T)\coth\alpha\kappa}, \quad \sigma_{p2}^2 = -\kappa. \tag{38}$$

Therefore, the asymptotic solution in the plastic phase will consist in a secondary periodic oscillation superimposed to a primary average behavior controlled by the linear combination of the exponentials $e^{\pm\sigma_{p1}\tau}$.

III. STABILITY BOUNDARIES

A. Average evolution of the perturbation amplitudes

As was shown in Refs. [31,41], a necessary condition for the stability of the system is that it has to be stable during the elastic phase; that is, it must be $\kappa \geqslant \kappa_c$ ($-\Omega^2 \equiv \sigma^2 < 0$). In such a case, the amplitude of the perturbation at the interfaces $y = 0$ and $y = -h$ will consist in a multimodal oscillation containing an infinite number of frequencies corresponding to the infinite roots of Eq. (32). As was first discussed by Plohr and Sharp [17], this is essentially because the dispersion relation goes asymptotically to infinity when $\alpha\sqrt{\kappa^2 - \Omega^2} = im\pi$, where m is an integer number. In such a case we have

$$\Omega^2 = \kappa^2 + \frac{m^2\pi^2}{\alpha^2}, \tag{39}$$

and, therefore, there is a root in between successive asymptotes for which $\Omega^2 \geqslant \kappa^2$. In addition, there is another root for which $\Omega^2 < \kappa^2$ that constitutes the smallest value of Ω^2. For instance, in the limit $\alpha \to \infty$ it is found $\Omega^2 = r^2\kappa^2$, where r^2 is the solution of the implicit equation $2(1+A_T)\sqrt{1-r^2} = r^2(1+\sqrt{1-r^2})$ ($r^2 = 0.9126$ for $A_T = 1$, and $r^2 = 0.7044$ for $A_T = 0$). Similar values are found from the numerical solution of Eq. (32) for finite α and $\kappa \gg \kappa_c$.

Therefore, we can consider that for $\kappa \geqslant \kappa_c$ the perturbation amplitudes at $y = 0$ and $y = -h$ can be written as the sum of an average oscillation determined by the lowest frequency, plus infinite superimposed oscillation modes of higher frequencies. For the present purposes, we will assume that only such an average amplitude of the perturbation determines the stability boundaries, and we consider all the higher frequencies as a kind of "noise" that cannot rule the bulk evolution of the instability. We notice that the numerical simulations reported in Ref. [8] displaying $\xi(t)$ widely support this assumption. This average perturbation amplitude of the interface at $y = 0$ will be the first to reach the boundary of plastic flow at the transition time t_T, and it will happen before it will achieve its absolute maximum. Thus, for times $t > t_T$ the slab is susceptible to be unstable.

On the other hand, for times shorter than the transition time t_T we will write the average amplitudes at $y = 0$ and $y = -h$, respectively, as follows ($t \leqslant t_T$):

$$z_a - 1 = (z_1 - 1)(1 - \cos\Omega\tau), \tag{40}$$

$$z_b = z_2(1 - \cos\Omega\tau), \tag{41}$$

where we have used the initial conditions given by Eq. (31), and Ω is now the smallest oscillation frequency given by Eq. (32). In addition, we have introduced the following definitions:

$$z_a = \frac{\xi_a}{\xi_0}, \quad z_b = \frac{\xi_b}{\xi_0}, \quad \tau = t\sqrt{k_0 g},$$
$$\Omega = i\sigma = \frac{\omega_e}{\sqrt{k_0 g}}, \quad z_1 - 1 = \frac{\ddot{\xi}_{a0}}{\xi_0\omega_e^2}, \quad z_2 = \frac{\ddot{\xi}_{b0}}{\xi_0\omega_e^2}. \tag{42}$$

The initial accelerations $\ddot{\xi}_{a0}$ and $\ddot{\xi}_{b0}$ are calculated from Eqs. (27) and (28) by solving at $t = 0$:

$$\frac{\ddot{\xi}_{b0}}{\ddot{\xi}_{a0}} = \frac{1}{\cosh\alpha\kappa}, \quad \frac{\ddot{\xi}_{a0}}{\xi_0\omega_e^2} = \frac{\sigma_{p1}^2}{\Omega^2\tanh\alpha\kappa}. \tag{43}$$

In a similar manner in the plastic phase ($t \geqslant t_T$) the average amplitude evolves governed by the growth rate σ_{p1} given by Eq. (38). For our purposes we need to pay attention only to the evolution of the interface at $y = 0$. Then, for $t \geqslant t_T$, we have

$$z_a = \frac{1+A_T}{2A_T}\frac{1}{\xi^*} + K_1 e^{\sigma_{p1}\tau} + K_2 e^{-\sigma_{p1}\tau}, \tag{44}$$

where the first term is a particular solution of Eq. (35) in dimensionless form, and

$$\xi^* = \frac{\rho_2 g\xi_0}{2Y}. \tag{45}$$

The constants K_1 and K_2 are determined by the matching conditions at the time $t = t_T$ with Eq. (40) for the elastic phase.

On the other hand, from Eqs. (27) and (35) we can find the plastic flow condition which yields the transition time t_T: $S'_{yy}(0) = 2Yk$. For this, we notice first that from Eqs. (40) and (41) we can write the following relationships:

$$\ddot{\xi}_{aT} - \ddot{\xi}_{a0} = \gamma_e^2(\xi_{aT} - \xi_{a0}), \tag{46}$$

$$\ddot{\xi}_{bT} - \ddot{\xi}_{b0} = \gamma_e^2(\xi_{bT} - \xi_{b0}), \tag{47}$$

where $\ddot{\xi}_b(t_T) = \ddot{\xi}_{bT}$ and $\ddot{\xi}_a(t_T) = \ddot{\xi}_{aT}$. Thus, the plastic flow condition at $y = 0$ can be written as follows:

$$2kG\xi_0[C(z_{aT} - 1) - Az_{bT}] = 2Y, \tag{48}$$

where

$$C = -\frac{2}{\Omega^2}[(\kappa^2-\Omega^2)\coth\alpha\kappa - \kappa\sqrt{\kappa^2-\Omega^2}\coth\alpha\sqrt{\kappa^2-\Omega^2}], \tag{49}$$

$$A = -\frac{2}{\Omega^2}[(\kappa^2-\Omega^2)\,\mathrm{csch}\,\alpha\kappa - \kappa\sqrt{\kappa^2-\Omega^2}\,\mathrm{csch}\,\alpha\sqrt{\kappa^2-\Omega^2}]. \tag{50}$$

In the previous equations we have used once again the definitions given by Eq. (33) and (42).

Then we rewrite Eq. (48) in terms of dimensionless magnitudes as follows:

$$C(z_{aT} - 1) - Az_{bT} = \frac{\lambda^*}{\xi^*}, \quad \lambda^* = \frac{\rho_2 g\lambda}{4\pi G} = \frac{1}{2\kappa}, \tag{51}$$

where $z_{aT} = z_a(t = t_T)$ and $z_{bT} = z_b(t = t_T)$.

Since $(z_1 - 1)$ and z_2 are particular solutions of Eqs. (27) and (28), its relationship can be written in terms of A and C as follows:

$$z_2 = \frac{A}{C + \lambda^*}(z_1 - 1). \tag{52}$$

Thus, Eq. (51) yields

$$z_{aT} - 1 = \frac{\lambda^*}{\xi^*}\frac{C + \lambda^*}{C^2 - A^2 + C\lambda^*}, \tag{53}$$

and the time $\tau_T = t_T/t_0$ for the transition to the plastic regime turns out as

$$\cos\Omega\tau_T = 1 - \frac{\lambda^*}{\xi^*}\frac{C + \lambda^*}{C^2 - A^2 + C\lambda^*}\frac{1}{z_1 - 1}. \tag{54}$$

Now we can calculate the constants K_1 and K_2 in Eq. (44) by matching it with Eq. (40) at $\tau = \tau_T$. For this, the continuity of z_{aT} and $\dot{z}_{aT}$ is imposed, yielding

$$1 + \frac{\lambda^*}{\xi^*}\frac{C + \lambda^*}{C^2 - A^2 + C\lambda^*} = \frac{1 + A_T}{2A_T}\frac{1}{\xi^*} + K_1 e^{\sigma_{p1}\tau_T} + K_2 e^{-\sigma_{p1}\tau_T}, \tag{55}$$

$$(z_1 - 1)\Omega\sin\Omega\tau_T = \sigma_{p1}[K_1 e^{\sigma_{p1}\tau_T} - K_2 e^{-\sigma_{p1}\tau_T}]. \tag{56}$$

By solving for K_1 and K_2, we get

$$2K_2 = 1 + \frac{\lambda^*}{\xi^*}\frac{C + \lambda^*}{C^2 - A^2 + C\lambda^*} - \frac{1 + A_T}{2A_T}\frac{1}{\xi^*} - (z_1 - 1)\frac{\Omega}{\sigma_{p1}}\sin\Omega\tau_T, \tag{57}$$

$$2K_1 = 1 + \frac{\lambda^*}{\xi^*}\frac{C + \lambda^*}{C^2 - A^2 + C\lambda^*} - \frac{1 + A_T}{2A_T}\frac{1}{\xi^*} + (z_1 - 1)\frac{\Omega}{\sigma_{p1}}\sin\Omega\tau_T. \tag{58}$$

B. Stability boundaries

As noticed in Ref. [31] the interface at $y = 0$ will be stable provided that the (average) amplitude ξ_a reaches an absolute maximum at a certain time $t = t_m \geqslant t_T$; that is, it will be stable if $\dot{\xi}_a(t_m) = 0$ and $\ddot{\xi}_a(t_m) \leqslant 0$. In other words, the conditions for marginal stability determining the stability boundaries read

$$\dot{z}_a(\tau_m) = 0, \quad \ddot{z}_a(\tau_m) = 0 \ (\tau_m \geqslant \tau_T). \tag{59}$$

These conditions are satisfied only when $K_2 = 0$, and then the following equation for the curve of marginal stability is obtained:

$$1 + \frac{1}{\xi^*}\left[\frac{\lambda^*(C + \lambda^*)}{C^2 - A^2 + C\lambda^*} - \frac{1 + A_T}{2A_T}\right] = \frac{\sigma_{p1}}{\Omega}\frac{\sin\Omega\tau_T}{\tanh\alpha\kappa}, \tag{60}$$

$$\sin\Omega\tau_T = \sqrt{1 - \left[1 - \frac{1}{\xi^*}\frac{\lambda^*(C + \lambda^*)}{(C^2 - A^2 + C\lambda^*)}\frac{\Omega}{\sigma_{p1}}\tanh\alpha\kappa\right]^2}, \tag{61}$$

where we have used Eq. (42) and (43) for expressing $(z_1 - 1)$, and $A = A(\lambda^*)$ and $C = C(\lambda^*)$ are given by Eqs. (49) and (50) [$\lambda^* = 1/(2\kappa)$].

Equation (60) can be rewritten as a quadratic equation for $\xi^* = \xi^*(\lambda^*)$ with α and A_T as parameters:

$$\xi^{*2} + F_1(\lambda^*)\xi^* + F_2(\lambda^*) = 0, \tag{62}$$

where

$$F_1(\lambda^*) = 2\left[H\left(1 - \frac{1}{\tanh\alpha\kappa}\right) - \frac{1 + A_T}{2A_T}\right], \tag{63}$$

$$F_2(\lambda^*) = \left(H - \frac{1 + A_T}{2A_T}\right)^2 + \left(\frac{H\Omega}{\sigma_{p1}}\right)^2, \tag{64}$$

with

$$H = \frac{\lambda^*(C + \lambda^*)}{C^2 + A^2 + C\lambda^*}, \tag{65}$$

σ_{p1} given by Eq. (38), and Ω being the smallest root of Eq. (32) for $\kappa \geqslant \kappa_c$.

Equation (62) completely determines the stability boundaries in the plane (ξ^*, λ^*) for the RTI in an accelerated EP solid slab, provided that it has already reached a regime in which it is accelerated as whole. Such a regime may be preceded by an early phase of Richtmyer-Meshkov instability and/or a transient phase in which a pressure wave is traveling inside the slab and it is not yet accelerated as a whole. In such cases, these previous phases will set the initial conditions for the late RTI phase.

C. Plastic flow boundaries

We can also calculate the boundaries for the EP transition by noticing that it must happen as the latest when the perturbation amplitude at $y = 0$, oscillating in the stable regime, reaches its maximum value:

$$z_a^{\max} - 1 = \frac{\ddot{\xi}_{a0}}{\xi_0 \omega_e^2} = z_{aT} - 1. \tag{66}$$

Then from Eqs. (43) and (53), we get

$$\xi^*_{\rm EP} = \frac{\tanh \alpha\kappa}{2} \left(\frac{\Omega}{\sigma_{p1}}\right)^2 \frac{\lambda^*(C+\lambda^*)}{C^2 + A^2 + C\lambda^*}, \tag{67}$$

where $\xi^*_{\rm EP}$ is the value of ξ^* for which the transition from the elastic to the plastic regime takes place.

IV. RESULTS OF THE THEORY AND DISCUSSION

A. Stability and plastic flow boundaries

We have represented in Fig. 2 the stability boundaries $\xi^*(\lambda^*)$ for the RTI in accelerated EP solids, such as given by Eqs. (62) to (65), as well as the corresponding boundaries $\xi^*_{\rm EP}(\lambda^*)$ for the EP transition given by Eq. (67), for three different values of the Atwood number: $A_T = 1$, 0.8, and 0.4, and for different values of the dimensionless thickness α of the slab.

For $A_T = 1$, Fig. 2(a) shows that, as could be expected, the stability region becomes smaller for the thinner slabs as a consequence of the reduction of the cutoff wavelength, in the elastic regime. In fact, this behavior was already predicted by the models of Refs. [12–15], and it was physically explained in Refs. [46,47]. Furthermore, it can be seen that the curves for the different values of α converge for small values of λ^*, which correspond to the limit of thick slabs, independently of the particular value of the slab thickness h. In addition, as was already found in Refs. [31,32] on the basis of an irrotational model, for $\lambda^* \to 0$, the dimensionless initial amplitude of the perturbation $\xi^* \to 1$, thus retrieving the Drucker's criterion [5,6].

In addition, the EP transition boundaries follow a similar tendency, always being below the stability boundaries, and reach a maximum value $\xi^{*\max}_{\rm EP} = 0.5$ for $\lambda^* = 0$ such as was found in Refs. [31,32] for semi-infinite media ($\alpha \gg 1$). It is interesting to notice that by considering that plastic flow was a sufficient condition for instability, the model of Refs. [11–14] artificially introduced a "correction factor" to force it to satisfy the Drucker's criterion for $\lambda^* = 0$, when they actually were dealing with the EP transition boundaries. However, without such a "correction factor," their model correctly predicts $\xi^{*\max}_{\rm EP} = 0.5$ (for $A_T = 1$).

For $A_T < 1$ [Figs. 2(b) and 2(c)], the results are qualitatively similar to the previous ones provided that α is above the critical value $\alpha^* = 2(1 - A_T)/A_T$, which determines the instability threshold below which the slab is stable in the elastic regime for *all* the perturbation wavelengths, such as was reported in Ref. [47] (see also Refs. [10,11,49,50]).

Below the instability threshold the change of the boundaries with α still follows the same tendency as for $A_T = 1$ for the smaller dimensionless wavelengths. But now the cutoff wavelength λ^*_c goes to infinity, though we have $\xi^*(\lambda^*) \to 0$ as $\lambda^* \to \infty$. This is the case of curves (a) in Figs. 2(a) and 2(b). That is, although the slab would be stable for any perturbation wavelength, the maximum amplitude allowed to remain below the stability boundaries decreases monotonically with λ^*.

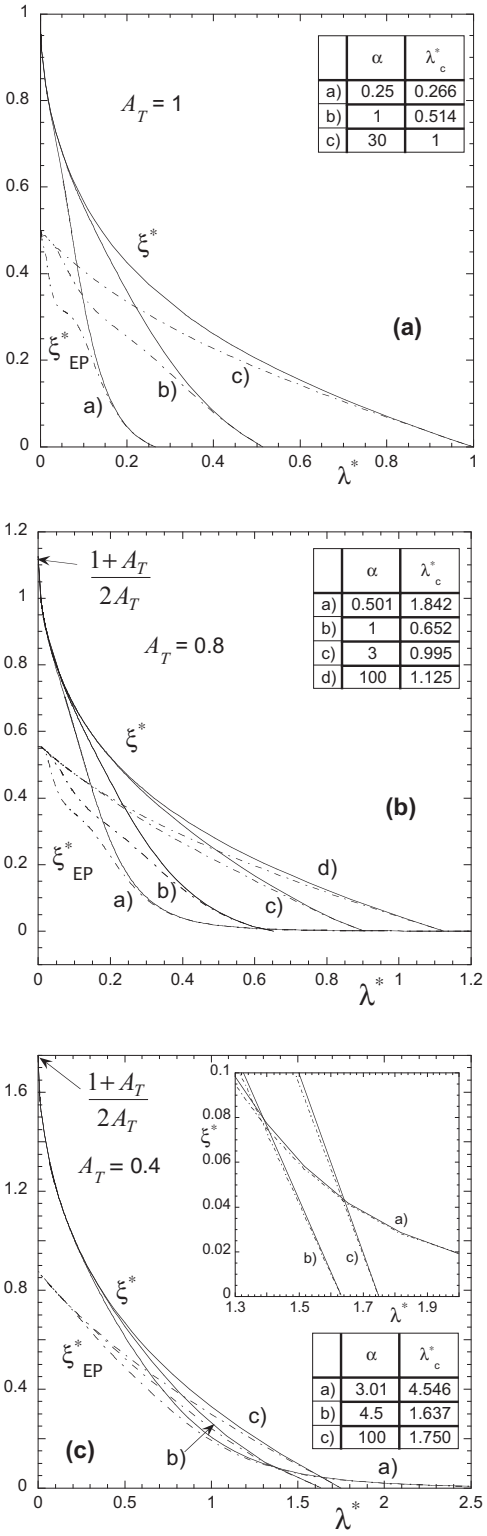

FIG. 2. Boundaries for stability (full lines) and for the elastic-plastic transition (dotted lines) for three values of the Atwood number and for different values of the parameter α indicated on the figures: (a) $A_T = 1$, (b) $A_T = 0.8$, and (c) $A_T = 0.4$.

Nevertheless, in practice, the maximum possible value of λ^* is limited by the lateral dimensions of the slab; for instance, it is the case of spherical or cylindrical shells for which the perimeter of the shells imposes the maximum possible perturbation wavelength.

On the other hand, the maximum value of ξ^* becomes higher for $A_T < 1$, and the maximum value of $\xi^*_{\rm EP}$ is always half of $\xi^{*\max}$(for $\lambda^* = 0$):

$$\xi^{*\max} = 2\xi^{*\max}_{\rm EP} = \frac{1+A_T}{2A_T}. \tag{68}$$

In summary, for $A_T < 1$, there exists the possibility to have total stability provided that the maximum perturbation amplitude can be made sufficiently small.

B. Some particular cases

We can better appreciate the previous facts with some particular examples. In Fig. 3 we show two particular cases corresponding to $A_T = 1$ and $A_T = 0.4$ [Figs. 3(a) and 3(b), respectively]. Figure 3(a) corresponds to the experiment reported in Ref. [22] of a cylindrical Al shell imploded by the magnetic pressure generated by a high-intensity pulsed current. In the figure we have also shown the values of the parameters we have taken for the calculations, some of which may not be very accurate because we had to infer them from the reported information, which may be somehow incomplete for our purposes. However, we think that the resulting picture is not far from the one corresponding to the experimental situation. As can be seen in Fig. 3(a) for $A_T = 1$, the stability boundaries are limited in the horizontal axis by a cutoff value $\lambda^*_c \approx 0.34$ that is much less than the maximum value $\lambda^{*\max} = 1.2$ determined by the size of the cylindrical shell, which would not allow for placing perturbation wavelengths larger than $2\pi R$ (where R is the radius of the cylinder). We have estimated a pretty good symmetry $\xi_0/h \approx 0.00025$, but since $\lambda^{*\max} > \lambda^*_c$, there is always a range of wavelengths that is out of the stable region in the stability map.

In Fig. 3(b) we show the case of the LAPLAS experiment that is being designed at the GSI Darmstadt (Germany) for performing experiments on HED physics driven by an intense heavy ion beam delivered by the new facility FAIR presently under construction [60–70]. According to the 2D numerical simulations, the maximum Atwood number during the implosion process is $A_T^{\max} \approx 0.4$, and the experiment will work below the instability threshold ($\alpha_{\rm LAPLAS} \approx 0.5 < \alpha^* \approx 3$). In addition, because of the relatively small size of the cylindrical shell, it is $\lambda^{*\max} \approx 0.7$, so that the experiment will remain within the stability boundaries provided that the symmetry level can be kept below 2%.

There are several differences between the liner driven by magnetic pressure and the one driven by heavy ion beams. But the fundamental one seems to be the possibility to keep the maximum Atwood number at a relatively small value in the latter case. This is a parameter that it is improbable that it can be modified in experiments with other drivers.

An exception, however, is the case of the shell implosions driven by the detonation products of HEs that are in contact with the shell, as in the experiments reported in Ref. [53]. These experiments seem to work in a very similar manner as the one foreseen for LAPLAS and consist in the implosion of a spherical shell of steel filled with a gas that is compressed during the implosion until its pressure stops the inward shell motion and a bounce is produced. At that moment the shell starts to move outwards (explosion phase). The shell is found to be perfectly stable during all the implosion process. But, instead, it becomes unstable after the bounce when the shell becomes accelerated outwards. In Fig. 4 we show the corresponding stability maps for the implosion [Fig. 4(a)] and the explosion [Fig. 4(b)] phases. The values of the parameters we have used for calculations are also indicated on the figure, and

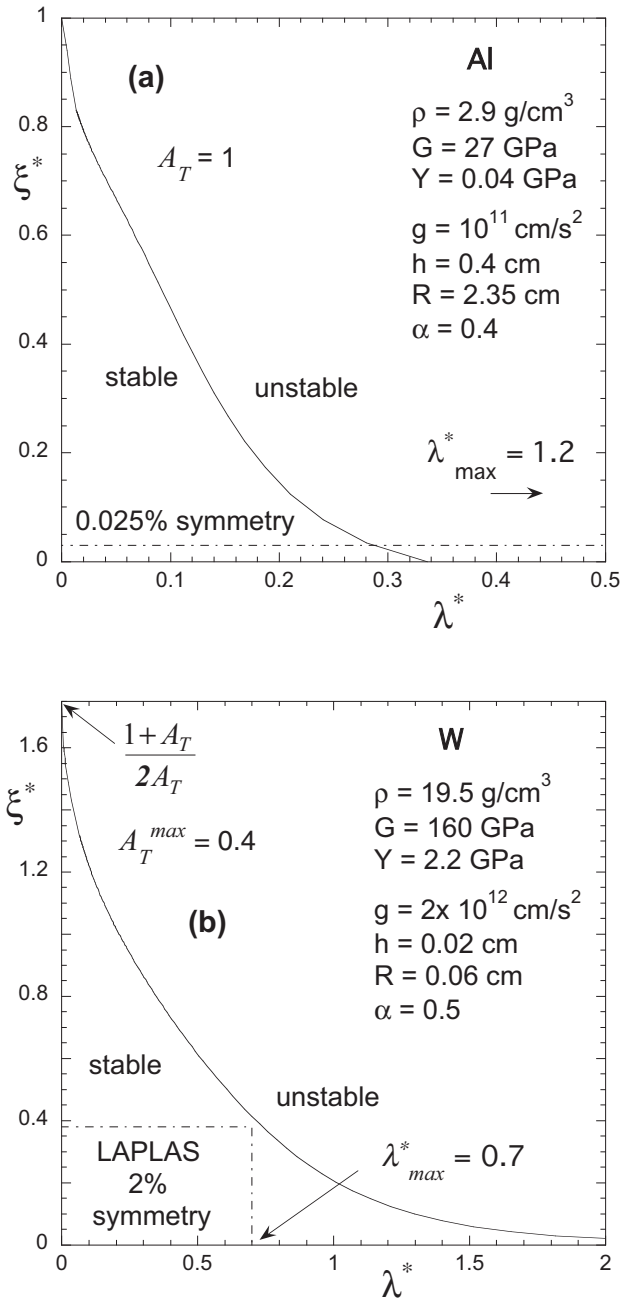

FIG. 3. Stability boundaries for two particular cases of cylindrical implosions: (a) driven by magnetic pressure [22], (b) driven by heavy ion beams [60–70].

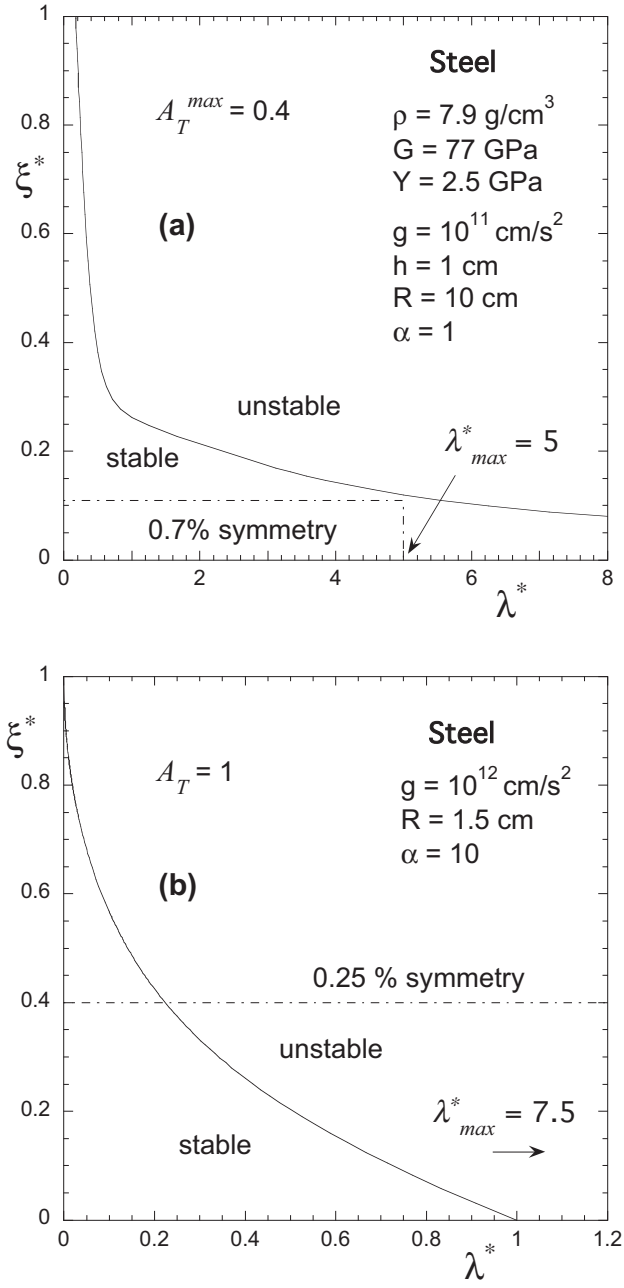

FIG. 4. Stability boundaries for a spherical shell driven by high explosives [53]: (a) implosion phase, (b) explosion phase.

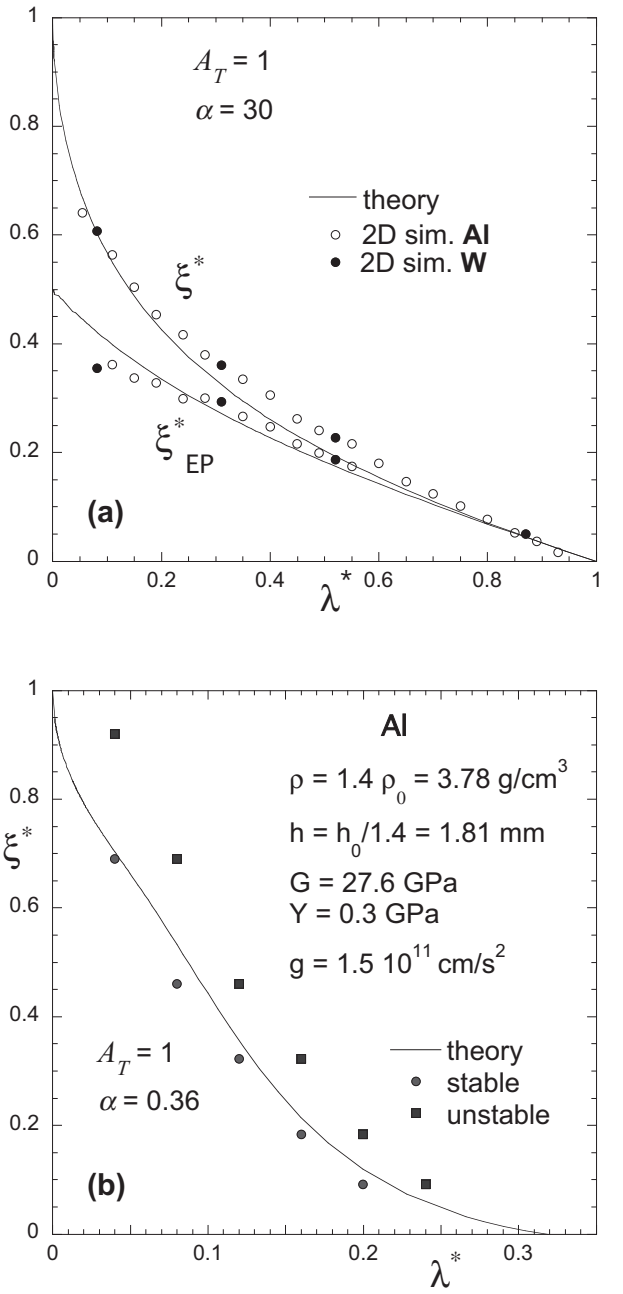

FIG. 5. Comparison with two-dimensional numerical simulations reported in the literature for $A_T = 1$: (a) stability and EP transition boundaries for W and Al thick slabs [31,32], (b) stability boundaries for the Barnes experiments [3,7], numerically determined in Ref. [6]. Full lines are the results of the present theory, and dots are from the simulations.

they are necessarily somewhat speculative because no many details are reported and we had to infer them according to our best knowledge.

However, we think that Fig. 4 illustrates the general physical scenario and can explain the experimental results. For the implosion phase [Fig. 4(a)] we have assumed a maximum Atwood number $A_T \approx 0.4$ and estimated a dimensionless thickness $\alpha \approx 1$, which results in being less than the corresponding instability threshold $\alpha^* = 3$. On the other hand, according to the size of the steel sphere, the maximum dimensionless wave number is $\lambda^* = 5$, so that stability is ensured if the symmetry ξ_0/h is better than 0.7%. This value corresponds to a surface finish of around 70 μm, which is well within the technologically achievable values.

During the explosion phase [Fig. 4(b)] the dimensionless shell thickness α considerably increases to $\alpha \approx 10$ essentially because of the increasing of the internal gas pressure ($\sim 10^3$ GPa), and it pushes further down the threshold value α^* for any reasonable value of the Atwood number that could be considered ($A_T > 0.6$, $\alpha^* < 1.33 < 10$). Then conservatively we have taken $A_T = 1$, for which the dimensionless cutoff

wave number is $\lambda_c^* = 1$, but conclusions are the same with any other reasonable choice [see curves (c) in Fig. 2]. However, for the minimum radius of the shell in this experiment it results in $\lambda^{*\max} \approx 7.5 \gg \lambda_c^*$; that is, there is always a wide range of perturbation wavelengths for which the exploding phase is unstable. In Fig. 4(b) we have also indicated, for reference, a symmetry level of 0.25%, which is probably beyond the present technological possibilities.

It is clearly seen that, because of the relatively high value of the parameter α in the explosion phase, there is a finite cutoff wave number, and it results in being less than the maximum wavelength that can exist in the shell perimeter. Therefore, the explosion phase will be unstable regardless of the quality of the interface surface finish.

C. Comparison with some existing 2D numerical simulations

It may also be worthwhile to compare the results of the present theory with some available 2D numerical simulations. In Fig. 5(a) we show the case of a very thick solid slab ($\alpha = 30$) and $A_T = 1$, which was modeled in Ref. [31,32] by means of an irrotational approximation. We have extracted the reported data for W and Al, and compared them with the present theoretical results, finding a very good agreement.

In Fig. 5(b) we have represented the data reported in Ref. [8] in which the experiments by Barnes *et al.* [3,7] were reproduced by means of 2D numerical simulations and a stability map was depicted. Here once again we had to make some inferences to supply the lacking information. As was previously mentioned, this is essentially because of the presence of an initial transient phase including the early development of the RM instability, a transient driving pressure, and the transit time of the pressure wave traveling into the slab until it becomes accelerated as a whole. We have assumed that during this transient phase the slab is compressed by a factor of around 1.4 but that the compression in the perturbation amplitude is more or less compensated by the instability growth during this transient. With $A_T = 1$ and the resulting value of $\alpha = 0.36$, the present theoretical results are fitted pretty well between the numerically determined unstable and stable cases.

V. CONCLUDING REMARKS

Based on a linear elastic perfect-plastic constitutive model for elastic-plastic solids, we have developed the 2D linear theory of the incompressible RTI in planar slabs. Then, by assuming that the bulk evolution of the instability is described by the growth of the average amplitude, we have determined the boundaries for stability and for plastic flow. Following Drucker [5,6], and the methods of limit analysis developed for soil plasticity [72,77], we have considered that RTI becomes dominated by plastic flow when plastic collapse occurs after the intermediate phase of contained plastic flow, and not just at the instant of impending plastic flow determined by the usual von Mises flow criterion.

As already shown in Refs. [31,32] for semi-infinite EP media, plastic flow is a necessary but not sufficient condition for instability. The stability is actually defined by the requirement that the perturbation amplitude reaches a maximum during the late plastic phase.

As a result it is found, as in the semi-infinite case, that the maximum (dimensionless) perturbation amplitude ξ^* is a decreasing function of the (dimensionless) perturbation wavelength λ^*, and both define the stability and the EP transition boundaries for the RTI in EP solids.

Since the maximum stable perturbation wavelength is given by the cutoff wavelength resulting in the elastic phase, there is a qualitative difference between situations with $A_T = 1$ and $A_T < 1$, since the latter case allows for the existence of an instability threshold below which elastic RTI is stable for any perturbation wavelength [10,11,47,49,50]. Then when $A_T < 1$ there exists the possibility to achieve complete stabilization provided that the initial perturbation amplitude is small enough.

Apart from the technological feasibility to reach a sufficiently good surface finish, to generate situations with $A_T < 1$ may lead to severe restrictions in the choice of the driver for accelerating the solid slab. At present, it seems to be possible only by using HEs in experiments in which the detonation products are close to the solid [53]. The theory presented here provides a reasonably coherent picture for explaining the experimental results.

The proposed experiment LAPLAS driven by heavy ion beams could share this feature in common with HE experiments, and it may represent a unique opportunity for novel experiments on HED physics. Also, in principle, it may offer the possibility to be scaled in the future to higher driver energies.

ACKNOWLEDGMENTS

This work has been partially supported by the Ministerio de Economía y Competitividad of Spain (Grants No. ENE2016-75703-R and No. BES-2017-079674), Junta de Comunidades de Castilla-La Mancha of Spain (Grant No. SBPLY/17/180501/000264), and the BMBF of Germany.

[1] J. W. Miles, Technical Report No. GAMD-7335, AD 643161, General Dynamics, 1966 (unpublished).
[2] G. N. White, Technical Report No. LA-5225-MS, Los Alamos National Laboratory, 1973 (unpublished).
[3] J. F. Barnes, P. J. Blewet, R. G. McQueen, K. A. Meyer, and D. Venable, J. Appl. Phys. **45**, 727 (1974).
[4] J. K. Dienes, Phys. Fluids **21**, 736 (1978).
[5] D. C. Drucker, in *Mechanics Today*, edited by S. Nemmat-Nasser (Pergamon, Oxford, 1980), Vol. 5, p. 37.
[6] D. C. Drucker, Ing.-Arch. **49**, 361 (1980).
[7] J. F. Barnes, D. H. Janney, R. K. London, K. A. Meyer, and D. H. Sharp, J. Appl. Phys. **51**, 4678 (1980).
[8] J. W. Swegle and A. C. Robinson, J. Appl. Phys. **66**, 2838 (1989).
[9] A. C. Robinson and J. W. Swegle, J. Appl. Phys. **66**, 2859 (1989).
[10] O. Blaes, R. Blandford, P. D. Madau, and P. Koonin, Astrophys. J. **363**, 612 (1990).

[11] O. Blaes, R. Blandford, P. D. Madau, and L. Yan, Astrophys. J. **399**, 634 (1992).

[12] P. N. Nizovtsev and V. A. Raevskii, VANT Ser. Teor. Prikl. Fizika **3**, 11 (1991).

[13] A. I. Lebedev, P. N. Nisovtsev, V. A. Rayevsky, in *Proceedings of the 4th International Workshop on the Physics of Compressible Turbulent Mixing (IWPCTM)* 29 March–1 April 1993, Cambridge, England (Cambridge University Press, Cambridge, England, 1993), p. 81.

[14] A. I. Lebedev, P. N. Nizovtsev, V. A. Raevskii, and V. P. Solovév, Phys. Dokl. **41**, 328 (1996).

[15] S. M. Bakhrakh, O. B. Drennov, N. P. Kovalev, A. I. Lebedev, E. E. Meshkov, A. L. Mikhailov, N. V. Neumerzhitsky, P. N. Nizovtsev, V. A. Rayevsky, G. P. Simonov, V. P. Solovyev, and I. G. Zhidov, Technical Report No. UCRL-CR-126710, Lawrence Livermore National Laboratory, 1997 (unpublished), https://www.osti.gov/scitech/servlets/purl/515973.

[16] E. L. Ruden and D. E. Bell, J. Appl. Phys. **82**, 163 (1997).

[17] B. J. Plohr and D. H. Sharp, Z. Angew. Math. Phys. **49**, 786 (1998).

[18] G. Dimonte, R. Gore, and M. Schneider, Phys. Rev. Lett. **80**, 1212 (1998).

[19] D. H. Kalantar, B. A. Remington, J. D. Colvin, K. O. Mikaelian, S. V. Weber, L. G. Wiley, J. S. Wark, A. Loveridge, A. M. Allen, A. A. Hauer, and M. A. Meyers, Phys. Plasmas **7**, 1999 (2000).

[20] C. A. Hall, J. R. Asay, M. D. Knudson, W. A. Stygar, R. B. Spielman, T. D. Pointon, D. B. Reisman, A. Toor, and R. C. Cauble, Rev. Sci. Instrum. **72**, 3587 (2001).

[21] J.-P. Davis, C. Deeney, M. D. Knudson, R. W. Lemke, T. D. Pointon, and D. E. Bliss, Phys. Plasmas **12**, 056310 (2005).

[22] R. E. Reinovsky, W. E. Anderson, W. L. Atchison, C. E. Ekdahl, R. J. Faehl, I. R. Lindemuth, D. V. Morgan, M. Murillo, J. L. Stokes, and J. S. Shlachter, IEEE Trans. Plasma Sci. **30**, 1764 (2002).

[23] J. D. Colvin, M. Legrand, B. A. Remington, G. Shurtz, and S. V. Weber, J. Appl. Phys. **93**, 5287 (2003).

[24] K. T. Lorenz, M. J. Eswards, S. G. Glendinning, A. F. Jankowski, J. McNaney, S. M. Pollaine, and B. A. Remington, Phys. Plasmas **12**, 056309 (2005).

[25] G. Terrones, Phys. Rev. E **71**, 036306 (2005).

[26] A. R. Piriz, J. J. López Cela, O. D. Cortazar, N. A. Tahir, and D. H. H. Hoffmann, Phys. Rev. E **72**, 056313 (2005).

[27] B. A. Remington, P. Allen, E. M. Bringa, J. Hawreliak, D. Ho, K. T. Lorenz, H. Lorenzana, J. M. McNaney, M. A. Meyers, S. W. Pollaine, K. Rosolankova, B. Sadik, M. S. Schneider, D. Swift, J. Wark, and B. Yaakobi, Mater. Sci. Tech. **22**, 474 (2006).

[28] A. R. Piriz, J. J. López Cela, N. A. Tahir, and D. H. H. Hoffmann, Phys. Rev. E **74**, 037301 (2006).

[29] J. J. López Cela, A. R. Piriz, M. C. Serna Moreno, N. A. Tahir, and D. H. H. Hoffmann, Laser Part. Beams **24**, 427 (2006).

[30] G. Terrones, J. Appl. Phys **102**, 034908 (2007).

[31] A. R. Piriz, J. J. López Cela, and N. A. Tahir, Phys. Rev. E **80**, 046305 (2009).

[32] A. R. Piriz, J. J. López Cela, and N. A. Tahir, J. Appl. Phys. **105**, 116101 (2009).

[33] H. S. Park, K. T. Lorenz, R. M. Cavallo, S. M. Pollaine, S. T. Prisbrey, R. E. Rudd, R. C. Becker, J. V. Bernier, and B. A. Remington, Phys. Rev. Lett. **104**, 135504 (2010).

[34] A. R. Piriz, J. J. López Cela, and N. A. Tahir, Phys. Rev. Lett. **105**, 179601 (2010).

[35] K. O. Mikaelian, Phys. Plasmas **17**, 092701 (2010).

[36] W. Gorczyk, B. Gobbs, and T. Gerya, Tectonophysics **514–517**, 146 (2012).

[37] W. Gorczyk and K. Vogt, Gondwana Res. **27**, 196 (2015).

[38] A. R. Piriz, Y. B. Sun, and N. A. Tahir, Phys. Rev. E **88**, 023026 (2013).

[39] A. R. Piriz, Y. B. Sun, and N. A. Tahir, Phys. Rev. E **89**, 063022 (2014).

[40] Y. B. Sun and A. R. Piriz, Phys. Plasmas **21**, 072708 (2014).

[41] S. Mora, T. Phou, J.-M. Fromental, and Y. Pomeau, Phys. Rev. Lett. **113**, 178301 (2014).

[42] A. R. Piriz, Y. B. Sun, and N. A. Tahir, Phys. Rev. E **91**, 033007 (2015).

[43] I. Maimouni, J. Goyon, E. Lac, T. Pringuey, J. Boujlel, X. Chateau, and P. Coussot, Phys. Rev. Lett. **116**, 154502 (2016).

[44] A. R. Piriz, Y. B. Sun, and N. A. Tahir, Eur. J. Phys. **38**, 015003 (2017)

[45] D. Riccobelli and P. Ciarletta, Philos. Trans. R. Soc. A **375**, 20160421 (2017).

[46] S. A. Piriz, A. R. Piriz, and N. A. Tahir, Phys. Rev. E **95**, 053108 (2017).

[47] S. A. Piriz, A. R. Piriz, and N. A. Tahir, Phys. Rev. E **96**, 063115 (2017).

[48] Y. B. Sun, J. J. Tao, and X. T. He, Phys. Rev. E **97**, 063109 (2018).

[49] S. A. Piriz, A. R. Piriz, and N. A. Tahir, Phys. Fluids **30**, 111703 (2018).

[50] S. A. Piriz, A. R. Piriz, and N. A. Tahir, J. Fluid Mech. **867**, 1012 (2019).

[51] R. Polavarapu, P. Roach, and A. Banerjee, Phys. Rev. E **99**, 053104 (2019).

[52] M. A. Meyers, *Dynamic Behavior of Materials* (John Wiley & Sons, New York, 1994).

[53] S. I. Blinnikov, R. I. Ilkaev, M. A. Mochalov, A. L. Mikhailov, I. L. Iosilevskiy, A. V. Yudin, S. I. Glazyrin, A. A. Golubev, V. K. Gryaznov, and S. V. Fortova, Phys. Rev. E **99**, 033102 (2019).

[54] J. Lindl, Phys. Plasmas **2**, 3933 (1995).

[55] A. R. Piriz, Phys. Fluids **31**, 658 (1988).

[56] A. R. Piriz and M. M. Sánchez, Phys. Plasmas **5**, 2721 (1998).

[57] J. R. Davies, D. H. Barnak, R. Betti, E. M. Campbell, P.-Y. Chang, A. B. Sefkow, K. J. Peterson, D. B. Sinars, and M. R. Weis, Phys. Plasmas **24**, 062701 (2017).

[58] S. Opie, E. Loomis, P. Peralta, T. Shimada, and R. P. Johnson, Phys. Rev. Lett. **118**, 195501 (2017).

[59] P. F. Knapp, M. R. Martin, D. H. Dolan, K. Cochrane, D. Dalton, J.-P. Davis, C. A. Jennings, G. P. Loisel, D. H. Romero, I. C. Smith, E. P. Yu, M. R. Weis, T. R. Mattsson, R. D. McBride, K. Peterson, J. Schwarz, and D. B. Sinars, Phys. Plasmas **24**, 042708 (2017).

[60] N. A. Tahir and D. H. H. Hoffmann, Phys. Plasmas **5**, 4426 (1998).

[61] A. R. Piriz, R. F. Portugues, N. A. Tahir, and D. H. H. Hoffmann, Phys. Rev. E **66**, 056403 (2002).

[62] N. A. Tahir, C. Deutsch, V. E. Fortov, V. Gryaznov, D. H. H. Hoffmann, M. Kulish, I. V. Lomonosov, V. Mintsev, P. Ni, D.

Nikolaev, A. R. Piriz, N. Shilkin, P. Spiller, A. Shutov, M. Temporal, V. Ternovoi, S. Udrea, and D. Varentsov, Phys. Rev. Lett. **95**, 035001 (2005).

[63] N. A. Tahir, A. Shutov, I. V. Lomonosov, A. R. Piriz, G. Wouchuk, C. Deutsch, D. H. H. Hoffmann, and V. E. Fortov, High Energy Density Phys. **2**, 21 (2006).

[64] N. A. Tahir, V. Kim, A. Matvechev, A. Ostrik, A. V. Shutov, I. V. Lomonosov, A. R. Piriz, J. J. López Cela, and D. H. H. Hoffmann, Nucl. Instr. Meth. B **245**, 85 (2006).

[65] N. A. Tahir, R. Schmidt, A. Shutov, I. V. Lomonosov, A. R. Piriz, D. H. H. Hoffmann, C. Deutsch, and V. E. Fortov, Phys. Rev. E **79**, 046410 (2009).

[66] N. A. Tahir, A. Shutov, A. P. Zharkov, A. R. Piriz, and Th. Stoehlker, Phys. Plasmas **18**, 032704 (2011).

[67] N. A. Tahir, I. V. Lomonosov, B. Borm, A. R. Piriz, A. Shutov, P. Neumayer, V. Bagnoud, and S. A. Piriz, Astrophys. J. Suppl. **232**, 1 (2017).

[68] N. A. Tahir, A. Shutov. I. V. Lomonosov, A. R. Piriz, P. Neumayer, V. Bagnoud, and S. A. Piriz, Astrophys. J. Suppl. **238**, 1 (2018).

[69] N. A. Tahir, P. Neumayer, A. Shutov, A. R. Piriz, I. V. Lomonosov, V. Bagnoud, S. A. Piriz, and C. Deutsch, Contrib. Plasma Phys. **59**, e201800143 (2019).

[70] N. A. Tahir, A. Shutov, A. R. Piriz, P. Neumayer, I. V. Lomonosov, V. Bagnoud, and S. A. Piriz, Contrib. Plasma Phys. **59**, e201800135 (2019).

[71] A. R. Piriz, J. J. López Cela, N. A. Tahir, and D. H. H. Hoffmann, Phys. Rev. E **78**, 056401 (2008).

[72] W. F. Chen, *Limit Analysis and Soil Plasticity* (Elsevier Scientific Publishing, Amsterdam, 1975).

[73] A. C. Eringen and E. S. Susuhi, *Elastodynamics. Vol. II: Linear Theory* (Academic Press, New York, 1975).

[74] K. S. Thorne and R. G. Blandford, *Modern Classical Physics* (Princeton University Press, Princeton, 2017), Chap. 12, pp. 629–642.

[75] V. N. Goncharov, P. McKenty, S. Skupsky, R. Betti, R. L. McCrory, and C. Cherfils-Clérouin, Phys. Plasmas **7**, 5118 (2000).

[76] M. E. Gurtin and L. Anand, J. Mech. Phys. Solids **53**, 1624 (2005).

[77] W. F. Chen and G. Y. Baladi, *Soil Plasticity. Theory and Implementation* (Elsevier Scientific Publishing, Amsterdam, 1985).

[78] K. O. Mikaelian, Phys. Rev. A **26**, 2140 (1982).

Correction: Equations (29), (30), (35), (36), (49), and (50) and an inline equation appearing before Eq. (46) contained typographical errors and have been set right.